



2nd International Conference on Structural Integrity, ICSI 2017, 4-7 September 2017, Funchal, Madeira, Portugal

Testing of Ultra-Low Cycle Fatigue at Complex Loading Scenarios

Sven Nagel^{a*}, Peter Knödel^a, Thomas Ummenhofer^a

^a*KIT Steel & Lightweight Structures, Research Center for Steel, Timber & Masonry, Karlsruhe (Germany)*

Abstract

This article describes systematic investigations on ULCF under multiaxial stress states and variable loading sequences as they occur under earthquake loading. The tests are performed on circular hollow sections (CHS) of structural steel S355 which are welded on baseplates. The multiaxial stress states are applied by bending respectively twisting the CHS, so that true strains up to 100 % per cycle and stress triaxialities between 0 and 0.6 occur. With this specimen and test setup arbitrary stress states in this range could be tested as well as predefined load sequences along different paths. In total 120 tests have been subjected to constant and variable amplitude loading. Different fracture modes and origins of fracture initiation have been observed. These experiments, their evaluation and documentation are presented within the article.

© 2017 The Authors. Published by Elsevier B.V.

Peer-review under responsibility of the Scientific Committee of ICSI 2017

Keywords: Earthquake Engineering; Variable Amplitudes; Plasticity; Ultra-Low Cycle Fatigue; Damage; Testing; Welded Structures;

1. Introduction

Structures subjected to earthquakes undergo irregular ground motions. These motions are transferred to the building itself in a way that frequencies and amplitudes are filtered by the dynamic behavior of the structure. Even in cases of simple static systems these motions can cause complex multiaxial stress states in structural components. As the aim of earthquake resistance design of structures is to reduce the seismic loads by adding or assigning certain regions as dissipative steel elements, large inelastic strains occur on purpose in such parts. These deformations appear in multiple

* Corresponding author. Tel.: +49 (0) 721 608 42207; fax: +49 (0) 721 608 44078.

E-mail address: sven.nagel@kit.edu

cycles with varying amplitudes. Current research proved the general dependency on the current stress state and termed the phenomenon of degradation caused by inelastic cyclic loading as ultra-low cycle fatigue (ULCF). Coupled as well as uncoupled micromechanical damage models based on the idea of void nucleation, growth and coalescence have been developed. The physical substantiation and mathematical implementation are based on single voids in infinite space [1, 2]. In further studies they have been expanded to realistic stress states and adapted for cyclic loading. Depending on the focus of the approaches, triaxiality time history, Lode's parameter evolution as well as accumulated plastic strains are considered [3, 4], [5]. In general the validity of advanced empirical approaches is limited to constant amplitudes and more restricting to the calibrated stress state, material properties and geometries [6],[7]. These models line up with specific component tests which are limited to the individual problem. Typically central notched tensile tests (CNT) are used to adapt distinctive stress triaxialities ($T \approx 0.4-1.7$) and investigate the fatigue behavior. The models are mostly calibrated to this small range of triaxialities which is accompanied by a fracture due to void formation [8]. Investigations on specimen for pure shear deformations ($T = 0$) or low triaxialities as for double notched specimens [4] are exceptions especially with respect to fatigue. The general validity of the micromechanical damage model needs to be questioned and proved for the whole range of stress states as these are mostly calibrated with the CNT and then extrapolated to lower triaxialities. Furthermore, experiments on steel specimen under monotonic loading at low triaxialities ($T \approx 0-0.2$) show big differences compared to the CNT range [8] for an aluminum alloy. Other studies [9] ($T = 0-1.6$) show a different behavior under monotonic loading for medium and high strength steels. Whether these differences are due to material behavior, characteristics in the stress states (such as the Lode parameter) or due to the type of loading could not be settled so far. In the event of an earthquake both situations occur: Complex multiaxial inelastic deformations meet the stress state and strain history dependent phenomenon of ULCF. To verify the resistance against this failure mode, most design codes help engineers by postulating plastic deformation limits or prescribe specific geometric situations. These strain limitations are a careful guess rather than based on material scientific facts. Therefore, investigations which cover the whole range of relevant stress states and its influence on the major characteristics of seismic loads are indispensable. This article summarizes experimental investigations, performed at the Karlsruhe Institute of Technology – Steel and Lightweight Structures (KIT) within the D-A-CH Project “ULCF of welded joints under variable multi-axial load” between Ecole Polytechnique Federale de Lausanne (EPFL), Graz University of Technology (TUG) and KIT. The aim of this project was to understand the ULCF behavior of welded joints of medium (S355) and high strength (S770) structural steel for a wide range of stress triaxialities. The investigations on material level [10, 11] are complemented by transient numerical simulations of unanchored tanks subjected to artificial acceleration time histories and loads of real seismic events [12]. This links the applied loading to realistic structural situations and shows the over conservative character of the EC design recommendations.

Nomenclature

T	stress triaxiality $T = \sigma_m / \sigma_{eq}$ with $\sigma_m = 1/3 (\sigma_1 + \sigma_2 + \sigma_3) / \sigma_{eq} = (1/2 ((\sigma_1 - \sigma_2)^2 + (\sigma_2 - \sigma_3)^2 + (\sigma_3 - \sigma_1)^2))^{0.5}$
L	Lode parameter
$\bar{\epsilon}_{pl}$	accumulated plastic strain
$\Delta \epsilon_p / 2$	plastic strain amplitude and $\Delta \epsilon_p / 2 = b (2N_f)^c$ Coffin-Manson law
$N_{reversals}$	two reversals are one Cycle

2. Methodology

2.1. Specimen

To achieve the aim of this project – understanding and quantifying the behaviour of welded steel parts under realistic earthquake loads – specimen and test setup needed to be designed accordingly.

The requirements for the investigations are defined as

- failure must occur by ULCF within 20 cycles or less
- investigations of welded connections
- coverage of a wide range of stress triaxialities
- application of constant and variable amplitude loading
- load paths defined by varying stress states and varying amplitudes need to be applicable.

For covering all these requirements it was necessary to achieve the different stress state by changing the characteristics of the applied load. This method varies from the well-known and established CNT-tests where the stress state is defined by the individual geometrical properties of the specimen. CHS welded to baseplates and subjected to bending forces and torques fulfill all defined requirements. As shown in Figure 1 schematically the loading of the specimen was applied by a predefined horizontal displacement (leading to a stress distribution of a cantilever beam) and an applied rotation around the tube's centreline (leading to a pure shear deformation in the tube). Applying a weighted combination of both, arbitrary stress states in the range of $T = 0$ to $T = 0.6$ are possible. Note: the cyclic loading causes constant stress-states with alternating signs, the documentation is limited to absolute values. To enforce the maximum strains and so the origin of the fracture under pure torsion at the area of the weld, the wall thickness of the tube was reduced in this area from the inside by 20 % as shown in the detail of Figure 1. For later evaluations the geometric discontinuity, the spot where the wall thickness increases, has special importance and is termed as geometric notch (GN). To cover most common construction steels, with respect to the yield strength, the material of the seamless fabricated CHS was chosen to be S355 J2H. Mechanical properties have been investigated at KIT according to ISO 148-1:2009 and ISO 6892-1:2009. R_{EH} , R_m , A are given in Table 1. For further numerical studies (not in the scope of this paper, to be published soon) cyclic tests on cone shaped LCF test specimens and digital image correlation system (DIC) supported tension tests, capturing uniform elongation and necking at high strains, to determine true stress-strain curves, have been performed. A material model consisting of both a Voce [13] and a Chaboche [14] approach, considering isotropic and kinematic hardening under cyclic loading listed as "Mod 1" in Table 1 has been calibrated.

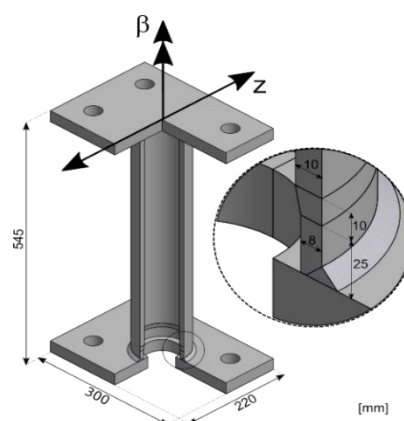


Figure 1: Tube-to-Plate specimen

Table 1: Parameters for Voce and Chaboche Model

	σ_0 [MPa]	C_1 [MPa]	γ_1	C_2 [MPa]	R_∞ [MPa]	b
Mod 1 ^a	352	6526	27.21	171	145	4
Mod 2 ^b	400	6526	27.21	171	70	50
	σ_0 [MPa]	R_m [MPa]	A [%]			
S355*	399 (7.33)	588 (3.50)	25.99 (1.04)			

* mean value & standard deviation of 7 tests on different CHS
^a Best fit from material tests ^b adopted for better fit to Tube-to-Plate tests

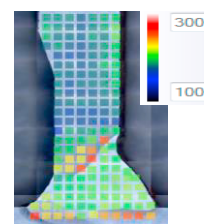


Figure 2: HV10 hardness mapping on a longitudinal section of the specimen

A welding procedure (WPS) for the assembling of the specimen has been developed. MAG 135 was used as welding process with a wire electrode 1.2 mm M G4Si1 [ISO 14341:2011]. The two-layer single bevel V weld was prepared with an angle of 45° and a gap of 2 mm and heated up to 150°C (200-220 A, 24-32 V with a travelling speed of 30 cm/min) which are the significant parameters regarding the welding residual stresses as shown in [15]. Macro polish and hardening tests (HV10 according to ISO 6507-1:2006) as well as a surface mapping presented in Figure 2 have been studied. Note: the notch in the weld toe is not representative for the tested specimens.

2.2. Test Setup

The theoretically defined head displacements and rotations, shown in Figure 1, were applied to the specimen by the test setup shown in Figure 3. Two jacks are placed horizontally and end up in a traverse which is connected to the top of the specimen. On the other side the jacks are attached to support columns. On either side of the jacks ball bearings allow motions in all directions with negligible friction. Both jacks are connected to a two-axis controller and equipped with internal displacement transducers. Force measuring sockets are attached to the piston rods. The applied deformations are controlled by simultaneous action of both jacks and are described with the help of the motion of a of a virtual reference point (RP). In the initial state RP is vertically aligned with the centreline of the jacks, in the horizontal plain it is placed in the centre of the tube and defines the origin of the illustrated coordinate system.

Translatory motion is applied by moving both jacks in the same direction simultaneously and pure torsion by moving them antimetric. Arbitrary combinations of torsion and bending are applied by different amplitudes and phases. The motion of the RP is not clearly defined by the two elongations of the jacks and therefore tracked by a DIC (DIC-global). Strains on the outer surface of the specimen in the area between the weld and the internal geometric notch, as explained in chapter 2.1, are measured by the help of a second DIC (DIC-local).

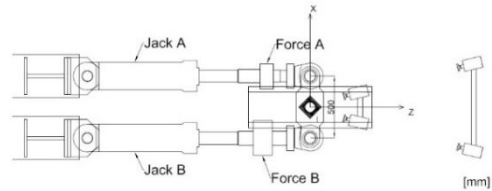
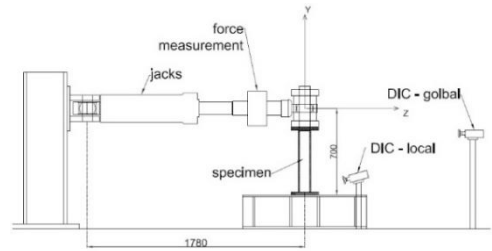


Figure 3: Test setup Tube-to-Plate

2.3. Test Matrix

96 of the 120 tested specimens are used for evaluation. The tests are classified in three major groups a) constant amplitudes, b) load paths and c) variable amplitudes. Each consists of several states as described below.

a) Constant stress states and constant amplitudes (CA)

Guided by pure bending ($k_\epsilon = 1$) and pure torsion ($k_\epsilon = 0$) four other load states in-between (termed “ratios”) have been tested. Two are dominated by bending, two by torsion. As the stress state is dominated by inelastic true strains up to 100 % these states were characterized by the strain relation k_ϵ defined in (1).

$$k_\epsilon = \frac{\epsilon_{axial}}{\epsilon_{axial} + \epsilon_{tangential}} \quad (1)$$

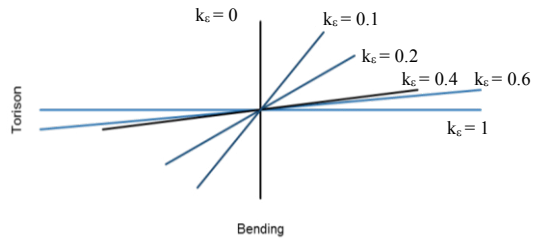


Figure 4: Qualitative load situations (see (1))

In the cases of $k_\epsilon = 1$ and $k_\epsilon = 0$ several magnitudes were applied. These magnitudes were chosen in a way, that either bending or head rotation of a ratio can be linked with one of these basic cases. The counterpart was added to this deformation. The tests are summarized in Figure 4 and Table 2. Informations of the stress state an strain amplitudes determined in numerical simulations with “Mod 2” are added.

Table 2: Test matrix CA

Code	k_ϵ	B [mm]	T [°]	T	L	$\Delta\epsilon_{pl}/2$
B 70	1	70	0	0.58	0.05	77
B 50	1	50	0	0.58	0	47
B 30	1	30	0	0.56	0	14
T 40	0	0	40	0	0	103
T 49	0	0	49	0	0	130

Code	k_ϵ	B [mm]	T [°]	T	L	$\Delta\epsilon_{pl}/2$
R 1.1	0.6	70	11	0.56	0.2	25
R 1.2	0.4	50	11	0.19	0.5	30
R 2.1	0.2	30	30	0.52	0.4	13
R 2.2	0.1	20	43	0.09	0.2	87

b) Path loading (P)

Four more complex scenarios termed as “path” were defined. These should cover realistic earthquake loading. In these cases, key stress states, represented by dots in Figure 5, are approached along different paths. The limiting states of pure bending and pure torsion are achieved in P1, P3 and P4 by mixed states, in P2 this transition is done continuously. Other than P3 and P4 the loading in P1 and P2 has alternating signs. For P1 and P2 two different amplitudes have been tested.

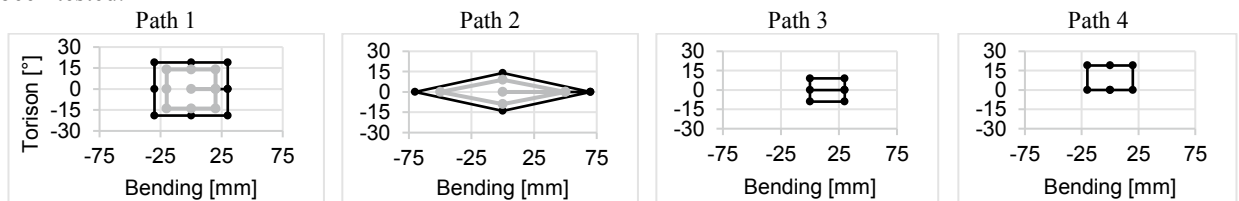


Figure 5: Overview of path loading with constant amplitudes

c) Tests with variable amplitudes (VA)

To face load sequence effects the amplitudes of a) and b) where combined using two time-series a) alternating, b) blocks of five constant amplitudes, as given in Table 3.

2.4. Evaluation

The elongation of both jacks combined with the acting forces have only very limited significance so that an extensive evaluation procedure was needed. First the forces and deflections have been separated into bending (shear and moment) and rotation (torque). Second the rotation leads to increasing normal forces within the traverse and needed to be excluded from the evaluation. Third the motion of RP is not clearly defined by the motion of the jacks. Tracking the spatial motions of the traverse on 8 points with a global DIC enables precise calculation of the RP during the loading. These 8 points were used as backup when a track was lost by the cameras within a test. The motion is split up into 3 translatoric and 3 rotatoric degrees of freedom and used for further numerical studies. The number of cycles to failure was defined to be marked by a drop in the forces by 10 % from the maximal value within the test. A catalogue of all fracture modes and surfaces was described and documented in pictures [16]. Strains on the surface in axial and horizontal direction where evaluated at five points between the geometric notch and the weld. These strains have been transferred according to [10] into equivalent strains. An uplift of the baseplate was significant in load cases dominated by bending and also tracked by the local DIC and used for the calibration of simulation models.

3. Results

3.1. Fracture modes

In contrast to [11] where fracture at similar specimens of S770 has exclusively been detected in the weld or its heat affected zone (HAZ), different origins and fracture modes have been observed with the KIT experiments. Far more often than having a weld failure the crack propagated from the inside of the tube starting in the GN. Table 4 illustrates the two major fracture origins which are termed as Mode I and II. More detailed differences in the fracture process have been defined for further reference.

Mode I a) – Fracture origin: GN – Loading: Bending

The fracture initialization is detected by an increase of the strain amplitude captured by the local DIC on the outer surface. At this moment no fracture is visible from outside and the bending force has not decreased significantly. This indicates the crack propagating from the inner to the outer surface. The defined fracture and so the drop in the force-displacement curve goes along with a necking of the wall thickness and crack opening. The fracture properties are summarized as: a) The vertical position of the crack remains constant and remains in the GN. b) The fracture surface indicates ductile behavior as it is characterized by shear lips and necking. c) The second hint for a crack initiation at the GN is a sharp line (may be a yield line) around the inner surface. This is expected being the plastic deformations around the GN.

Mode I b) – Fracture origin: GN – Loading: Torsion

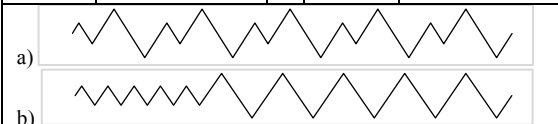
Fracture initialization occurs after changing the direction of the rotation. In this case the crack starts at an arbitrary circumferential position in the height of the GN. A pronounced sliding plane concentrating huge plastic deformations is observed within the reduced wall thickness of the tube. Fracture itself and so the drop in the force-displacement curve is abrupt and mostly accompanied by a pop.

Mode II a) – Fracture origin: HAZ – Loading: Bending / Ratio

Large strains are indicated by chipping off of the DIC paint in the weld seam transition. The propagation in circumferential direction takes place within seconds. Other than for mode I a) it is a more brittle fracture, no necking occurs and the drop in the force-displacement curve is more abrupt.

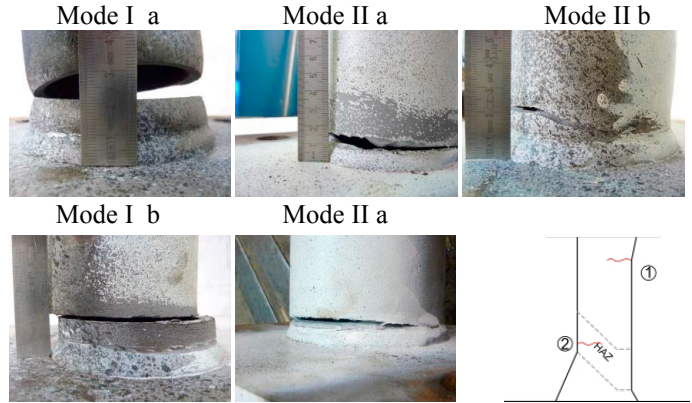
Table 3: Variable amplitude loading

Code	Combination of	Code	Combination of
VA B	B50 & B70	VA P1	P1.1 & P1.2
VA T	T40 & T49	VA P2	P2.1 & P2.2
VA R 1	R1.1 & R1.2	VA P3	P3 & P1.2
VA R 2	R2.1 & R2.2	VA P4	P3 & P1.2



In most of the bending dominated ratios the crack is initiated in the HAZ. In this area the fracture surface is orientated nearly perpendicular to the tube surface. After propagating for about 120° of circumference in the HAZ the crack switches into the base material and even through the geometric notch. Hereby the fracture surface changes its angle to 30-45° from its original orientation.

Table 4: Overview of different fracture origins and modes



Mode II b) – Fracture origin: HAZ – Loading: Torsion

The characteristic (brittle failure) is similar to the fracture according to Mode I b) but the origin is in the HAZ and the crack propagates into the base material along an angle of 30°.

3.2. Load paths and variable amplitudes

The evaluation and description of the load paths and variable amplitude tests underline the influence of the stress states and suggest a dominating dependency on the path between the states. While this paper concentrated on the description of the tests and the evaluation procedure, more elaborated findings on the material behaviour will be published after finishing the combined evaluation of numerical investigations.

3.3. Influence of the stress states

The first results are in line with the findings for monotonic loading in [9] and show the influence of the stress state on the ULCF-resistance. Limiting the evaluation to a phenomenological approach the influence is as summarized in Table 5 for constant amplitude loading. Three pairs of situations, each characterized by the same bending amplitude, are highlighted. In all cases the mean value of number of reversals to failure ($N_{rev, fail, mean}$) for a group of tests with the same loading situations are used for evaluation. Reducing k_ϵ by adding an additional shear component, $N_{rev, fail, mean}$ increases by up to 265 % compared to the tests under pure bending. For shear dominated ratios the increase is lower. An example is given in Figure 6.

Table 5: influence of the stress state on the tests results

Bending Amplitude	Bending $N_{rev, fail, mean}$	Ratio $N_{rev, fail, mean}$	k_ϵ	Increase of N_{fail}
30 mm	40	46	0.2	16 %
50 mm	14	51	0.4	263 %
70 mm	5	18	0.6	265 %

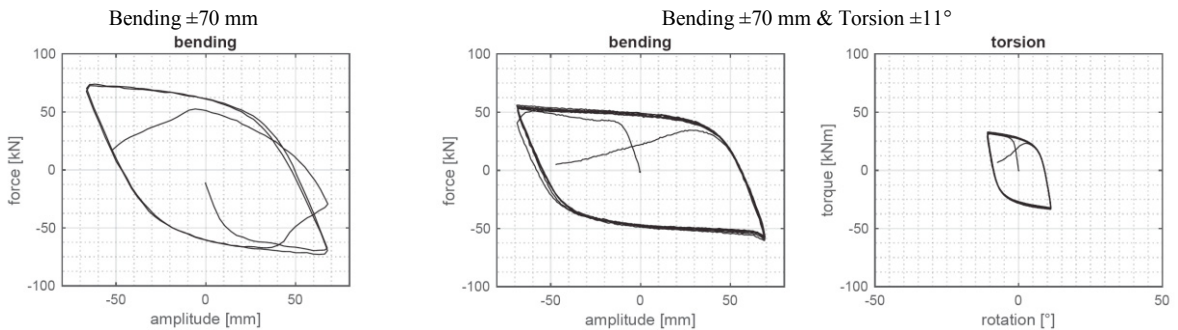


Figure 6: Comparison of force-displacement and torque-rotation plots for 70 mm bending amplitude and left: $k_\epsilon = 0$ and right: $k_\epsilon = 0.2$.

3.4. Characterizing lifetime-curves

Strain based considerations confirm the phenomenological findings. Considering the origins of fracture discussed in 3.1, a direct transfer from the DIC data to the damage relevant strains as done in [11] is not possible. The damage hotspot and origin of fracture is not captured by the DIC as it is located in the inner side of the tube. A transfer from the strains on the outer surface at the same distance from the baseplate is not purposeful due to the different characteristics of the strain fields shown for the two limiting cases, pure bending and pure torsion, in Figure 7. To solve this problem, numerical simulations with tiny elements ($l_{elem} < 0.2$ mm) in both the weld and the GN for all load scenarios have been performed. After evaluating the strain relation on the inner and outer surface, assumed strains on the inside could be determined from the measured strains on the outside. These assumed strains were used to plot lifetime curves in Figure 8. Within these simulations an immense influence of the material and simulation model was observed so that two limiting conditions (red – Mod 1 / black – Mod 2) were defined. In both cases a pronounced influence of the stress state is found and highlighted with two Coffin-Manson laws, the bending dominated (solid line) and shear dominated (dashed line). The associated parameters are (Mod 1 bending $b = 0.6 / c = -0.5$) (Mod 1 torsion $b = 25.4 / c = -1.2$) (Mod 2 bending $b = 2.8 / c = -0.8$) (Mod 2 torsion $b = 71.8 / c = -1.4$). Considering the accumulated plastic strain at fracture in Figure 9 both the big influence on the material model as well as on the stress states becomes more obvious. An extrapolation of the data to lower amplitudes, the theoretical intersection of bending and shear dominated curves and further validation of the material models are topic of current research.

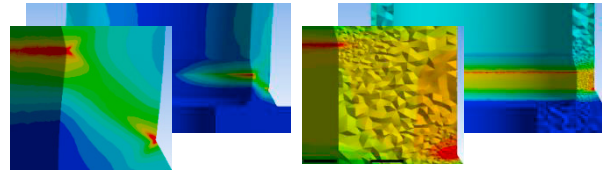


Figure 7: Plastic strain fields for left: pure bending right: pure torsion, in Figure 7. To solve this problem, numerical simulations with tiny elements ($l_{elem} < 0.2$ mm) in both the weld and the GN for all load scenarios have been performed. After evaluating the strain relation on the inner and outer surface, assumed strains on the inside could be determined from the measured strains on the outside. These assumed strains were used to plot lifetime curves in Figure 8. Within these simulations an immense influence of the material and simulation model was observed so that two limiting conditions (red – Mod 1 / black – Mod 2) were defined. In both cases a pronounced influence of the stress state is found and highlighted with two Coffin-Manson laws, the bending dominated (solid line) and shear dominated (dashed line). The associated parameters are (Mod 1 bending $b = 0.6 / c = -0.5$) (Mod 1 torsion $b = 25.4 / c = -1.2$) (Mod 2 bending $b = 2.8 / c = -0.8$) (Mod 2 torsion $b = 71.8 / c = -1.4$). Considering the accumulated plastic strain at fracture in Figure 9 both the big influence on the material model as well as on the stress states becomes more obvious. An extrapolation of the data to lower amplitudes, the theoretical intersection of bending and shear dominated curves and further validation of the material models are topic of current research.

4. Conclusions

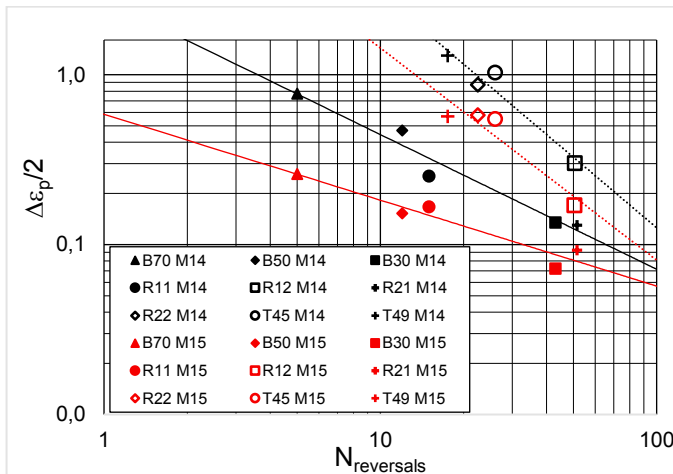


Figure 8: Lifetime curves of assumed strains, derived from combined evaluation of numerical and test data

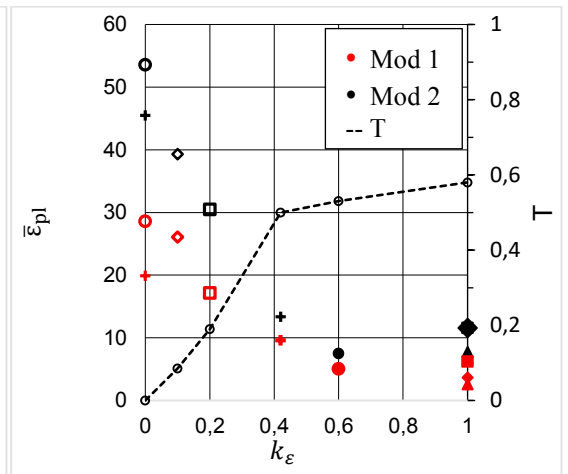


Figure 9: Accumulated plastic strains depending on the stress state and material model

CHS welded to base-plates and loaded by bending and torsion provide appropriate specimen to investigate a wide range of stress states at constant and variable amplitudes as well as more complex load scenarios under cyclic inelastic deformations. In the cases of S355 the influence of the geometric discontinuity is more pronounced compared to S770 of [11] and dominates the fracture. Investigations of the weld could only be done on a limited number of specimens. Nevertheless material subjected to ULCF has been investigated and the influence of the stress states on the ULCF-resistance is in line with the monotonic tests of [9]. Compared to [11] where similar tests were done for S770 the influence of the stress states is more pronounced for the S355. The Coffin-Manson law for tests with high stress triaxialities fit to the experiences of structural steel and represent a conservative limitation for design. High reserves

could be used for more economic design at shear dominated stress states and large strain amplitudes. Further extensive numerical investigations are needed to evaluate the tests. Their background, results and a classifications of the results in the context of the D-A-CH-Project (comparison of medium and high strength steels and the application to design guides) will be published soon.

5. Acknowledgments

The authors would like to thank their project partners from EPFL and TUG for the pleasant cooperation and the Deutsche Forschungsgemeinschaft (DFG) for the financial support.

6. References

- [1] McClintock, F. A. *A criterion for ductile fracture by the growth of holes*. Journal of Applied Mechanics 35 (1968), pp. 363–371.
- [2] Rice, J. R.; Tracey, D. M. *On the ductile enlargement of voids in triaxial stress fields*. Journal of the Mechanics and Physics of Solids 17 (1969), pp. 201–217.
- [3] Kanvinde, A. M.; Deierlein, G. G. *Cyclic Void Growth Model to Assess Ductile Fracture Initiation in Structural Steels due to Ultra Low Cycle Fatigue*. International Journal of Fatigue 132 (2006), pp. 1907–1918.
- [4] Smith, C. M.; Deierlein, G.; Kanvinde, A. M. *A Stress-Weighted Damage Model for ductile fracture initiation in structural steel under cyclic loading and generalized stress states*. Technical Report 187, Stanford University, John A. Blume Earthquake Engineering Center, California, 2014.
- [5] Ohata, M.; Toyoda, M. *Damage concept for evaluation ductile cracking of steel structure subjected to large-scale cyclic straining*. Science and Technology of Advanced Materials 5 (2004), pp. 241–249.
- [6] Kuroda, M. *Extremely low cycle fatigue life prediction based on a new cumulative fatigue damage model*. International Journal of Fatigue 24 (2001), pp. 699–703.
- [7] Xue, L. *A unified expression for low cycle fatigue and extremely low cycle fatigue and its implication for monotonic loading*. International Journal of Solids and Structures 30 (2008), pp. 1691–1698.
- [8] Bao, Y.; Wierzbicki, T. *On fracture locus in the equivalent strain and stress triaxiality space*. International Journal of Mechanical Sciences 46 (2004), pp. 81–98.
- [9] Faleskog, J.; Barsoum, I. *Tension-torsion fracture experiments - Part I: Experiments and a procedure to evaluate the equivalent plastic strain*. International Journal of Solids and Structures 50 (2013), pp. 4241–4257.
- [10] de Castro e Sousa, Albano; Nussbaumer, A. *Ultra low cycle fatigue of welded steel joints under multiaxial loading*. 6th International Conference on Structural Engineering, Mechanics and Computation, Cape Town, South Africa, 2016.
- [11] de Castro e Sousa, Albano. *Ultra low cycle fatigue of welded steel joints under multiaxial loading*. PhD thesis, École Polytechnique Fédéral de Lausanne, Resslerab, Lausanne, 2017.
- [12] Tappauf, C.; Taras, A. *Deformation and Strain Histories in Shell-to-Base Joints of Unanchored Steel Storage-Tanks During Seismic Loading*. 8th International Conference on Behaviour of Steel Structures in Seismic Areas, Shanghai, China, 2015.
- [13] Voce, E. *The relationship between stress and strain for homogeneous deformation*. Journal of the Institute of Metals 74 (1948), pp. 537–562.
- [14] Chaboche, J. L.; Rousselier, G. *On the Plastic and Viscoplastic Constitutive Equations - Part I: Rules Developed With Internal Variable Concept*. Journal of Pressure Vessel Technology 105 (1983), pp. 153–158.
- [15] Knödel, P.; Gkatzogiannis, S.; Ummenhofer, T. *Practical aspects of welding residual stress simulation*. Journal of Constructional Steel Research 132 (2017), pp. 83–96.
- [16] Ummenhofer, T.; Knödel, P.; Nagel, S. et al. *Ultra-Low Cycle Fatigue of welded joints under variable, multi-axial strains*. Documentation on D-A-CH research project. Supported by Deutsche Forschungsgemeinschaft (DFG), Karlsruhe Institute of Technology, Research Center for Steel, Timber & Masonry, Karlsruhe, 2017.